J. Fluid Mech. (2000), *vol.* 410, *pp.* 185–210. Printed in the United Kingdom

Thread-annular flow in vertical pipes

By Ch. FREI, P. LÜSCHER AND E. WINTERMANTEL

Biocompatible Materials Science and Engineering, Swiss Federal Institute of Technology, Zurich, Switzerland

(Received 28 September 1998 and in revised form 17 November 1999)

Thread injection is a promising method for different minimally invasive medical applications. This paper documents an experimental study dealing with an axially moving thread in annular pipe flow. Mass flow and axial force on the thread are measured for a 0.46 mm diameter thread in pipes with diameters between 0.55 and 1.35 mm. The experiments with thread velocities of up to 1.5 m s^{-1} confirm the findings of theoretical studies that for clinical requirements the radius ratio between thread and pipe is crucial for the adjustments of mass flow and force on the thread.

In both regimes, laminar and turbulent flow, the thread shows a characteristic oscillatory behaviour without touching the pipe wall. Resonance-like oscillations indicate circular thread motions around the pipe centre. The oscillating eccentricities may arise from longitudinal inhomogeneities of the thread shape and flow disturbances which cause non-stationary lateral momenta. According to established findings on annular flow with eccentric cylinders we assume that the mass flow, which is high compared to the concentric model, is caused by the temporary thread eccentricities. These findings should be considered in clinical applications to avoid possible thread blockage due to resonance-like vibrations.

1. Introduction

In implant surgery, porous medical implants are often desired to enable the ingrowth of blood vessels and cells. Contemporary porous implants, however, require invasive surgery. An aim of research is to reduce surgical trauma by designing minimally invasive implants. A thread tangle has a porous structure, and we have found a method to place this implant in a minimally invasive way (Lüscher, Winter-mantel & Annen 1995) called *thread injection*; it is illustrated in figure 1. Initially, a single thread is stored on a spool inside a fluid container, with one end introduced into a small-diameter pipe. The end of the pipe is put into the body in a minimally invasive way. By pressurizing the fluid container the thread is transported along with the fluid through the pipe, and at the exit forms the desired porous tangle inside the body tissue.

The coherent thread structure enables the transport of solid materials through any tube, catheter, or cannula with a small diameter. The injected implant volume is not restricted and can be adjusted to the clinical needs. The possibility of using different carrier fluids and combining different medical implant materials and thread types – such as mono- or multifilaments – opens up a wide range of applications: implants inducing the ingrowth of tissue, drug delivery systems, therapeutic embolization of blood vessels, or cavity filling after surgery.

The aim of this paper is to give some experimental insight into the fluid-dynamic effects of *thread-annular flow* where only the flow situation inside the pipe is considered. On the basis of these empirical results, the important parameters for future

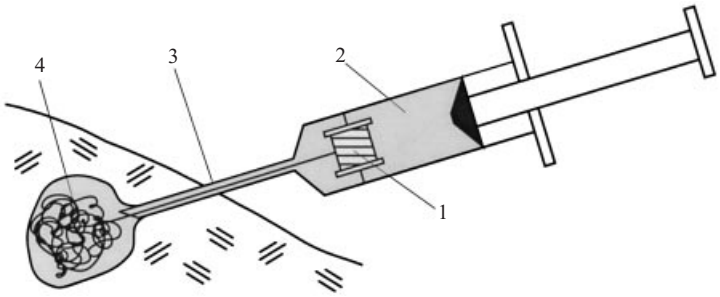

FIGURE 1. Principle of thread injection: the thread is stored on a spool (1) inside a fluid container (2). Through the injection pipe (3) the thread is brought to the site of interest inside the body in a minimally invasive way when pressure is applied in the fluid container. At the exit the desired porous tangle (4) is formed.

optimization of the device mentioned above are uncovered. These parameters, i.e. the pressure gradient over the pipe length, the geometry of the annular flow channel, and the thread velocity, are incorporated into a flow model.

In medical applications, the reliability of the system and the total fluid volume injected into the body are crucial values. Reliability is increased by a large propelling force on the thread in the flow direction as it allows resistive forces that may interrupt the injecting process to be overcome. Our measurements reveal how the axial force on the thread, which we call the thread force, is affected by flow parameters. The adjustment of the injected fluid volume directly correlates with the control of the mass flow. In these experiments this relation is investigated in the form of the friction factor. Lateral deviations of the non-rigid thread may occur due to flow inhomogeneities. Thread vibrations thus may lead to a mean eccentric position of the thread. For the study of thread forces and friction factor this eccentricity is taken into account as an additional parameter.

An example of thread injection is found in textile weaving where the weaving thread is introduced by an air stream through a pipe into the weaving process (Krause 1988). With Mach numbers of at least 0.3, the flow is highly turbulent, and the fluid has to be considered a compressible medium (Sabit & Mohamed 1991). High fluid velocities like that, however, are not acceptable in medical applications where mostly aqueous, incompressible solutions are involved, and laminar flow is expected to prevail. Results from textile engineering cannot therefore be directly transferred to thread-annular flow.

Other findings on transportation in liquid pipe flows and multiphase flows, however, are more comparable to thread-annular flow. They can be separated into annular flow types with axially fixed and axially moving cores.

1.1. *Fluid-dynamic investigations of annular pipe flow with fixed cores*

Axially fixed cores are the subject of various studies on flow in a pipe containing a rigid cylinder of circular cross-section. This flow situation is analogous to the initial phase of thread injection where the thread is not yet moving in the axial direction, but fluid-dynamic forces are accelerating it.

Piercy, Hooper & Winny (1933) found that increasing the ratio between the core and the pipe radius increases the axial traction on the core and pipe for the concentric laminar flow configuration; in addition, Koch & Feind (1958) calculated an increase of the friction factor. Experiments confirmed that increasing the radius ratio subsequently

leads to a reduction of the flow rate. According to Snyder & Goldstein (1965), shear stress variations arise on the circumference of the pipe and core wall when the core is displaced from the concentric position. When this eccentricity was increased an increased annular flow rate resulted from the laminar models of Piercy *et al.* (1933) and Redberger & Charles (1962) which corresponds to the decrease in the friction factor revealed by Tiedt (1968).

Generally, in turbulent flow the same tendencies of variations in radius ratio and eccentricity were observed as in laminar flow (Eifler & Nijsing 1971; Jonsson 1966). Koch & Feind (1958), however, discovered that in a concentric annulus the transition from laminar to turbulent flow takes place at Reynolds numbers betweeen 3000 and 4000, which are higher than in pipe flow. In their turbulent models, Nelson & Robertson (1968) and Indelkofer (1981) took additional parameters into consideration, such as wall roughness and eccentricity.

1.2. *Moving cores in pipe flow*

Another flow type to be considered is pipe flow with a rigid cylinder moving in the axial direction, which is comparable to a running thread injection. For concentric annular flow Shigechi & Lee (1991) calculated a decrease of the friction factor with increasing axial core velocity. At the same time the increasing effect of the radius ratio is maintained in this flow situation. Generally, eccentricity affects the friction factor obtained by the analytical solution of Shigechi, Momoki & Lee (1994) in the same decreasing way as in the case with a fixed core. At very high core velocities, however, it was observed that the friction factor was increased by the eccentric position of the core. In the turbulent model for concentric annular flow with axially moving core Shigechi, Kawae & Lee (1990) derived analogous influences of the parameters as in the laminar flow. Shear forces on the core surface which result in an axial force component were not considered in these investigations. In addition, no experimental data are given that would for instance allow to discuss the influence of the core velocity on the transition range from laminar to turbulent flow.

1.3. *Lateral core deviations and vibrations in annular flow*

Oscillations and instabilities affect many annular flow types with rigid cores. In laminar concentric annular flow Piercy *et al.* (1933) detected sinuous waves in the tangential direction. Vibrations in heat exchangers with pipes subjected to parallel or axial flow are a common problem in practice. A general introduction to the stability of cylinders in axial flow is given by Chen (1987). Unstable cylinder responses, such as divergence or flutter, were found only to appear due to very large turbulent fluid velocities which are irrelevant in most practical applications. For lower turbulent flow velocities, stable vibrations of flexible cylinders with restricted lengths are investigated by different authors (Chen & Wambsganss 1972; Paidoussis 1966*a*, *b*, 1973).

Thorough research on vibrations and instabilities has been conducted regarding core-annular flow where the major problem is to achieve a stable multiphase flow with water at the pipe wall completely surrounding and lubricating an oil core. This principle is applied in pipelining of heavy crude oils. Most instabilities of this flow type, such as interfacial instabilities (Hu & Joseph 1989), hardly affect thread-annular flow. Transient rotating corkscrew waves, however, as observed by Bai, Chen & Joseph (1992), could also occur in the thread-annular flow. In those experiments buoyancy caused a resistance force on the core in down-flow similar to the resistance force in thread-annular flow deriving from the spool. Ooms, Segal & Van Der Wees (1984), and Bai, Kelkar & Joseph (1996) showed that ripples observed on the oil–

water interface could generate pressure variations in the annulus that counterbalance buoyancy and prevent the core from touching the wall. Rough surface topographies such as on multifilament threads could cause similar effects.

1.4. *Relevance of the literature to thread-annular flow*

The literature discussed above reveals that there are no specific models and experiments for thread-annular flow with a liquid as transport fluid. In particular, hardly any experimental data about annular flow with an axially moving inner core are available. It is therefore necessary to conduct experiments on thread-annular flow and to check the applicability of the existing models.

In this study, the explicit model of Shigechi & Lee (1991) for a concentric annular flow with a moving rigid core is used to approximate the laminar thread-annular flow. A high-viscosity fluid core like in core-annular flow could serve as another model for the flexible thread in axial pipe flow. This model is not analytically evaluated in these investigations, but taken into account in a qualitative discussion. The turbulent models mentioned above may also be relevant for thread injection; in medical applications, however, the corresponding high mass flows are rarely acceptable. The discussion on turbulence is therefore solely based on simple empiric correlations.

Our experiments show that in thread-annular flow there are vibrations and lateral deviations of the thread. Comparisons with findings of vibrations and instabilities of fixed rigid cores and fluid cores in core-annular flow may in future enable the development of a specific fluid-dynamic model for instabilities and vibrations in thread-annular flow. A model of this kind could predict different types of vibration, and, subsequently, the influence on mass flow, friction factor, and thread force.

If the vibrational models of solid cylinders of restricted length were applied to thread-annular flow different end conditions would have to be considered. In contrast to cylinders with fixed–fixed, fixed–free or pinned–pinned ends, the thread in pipe flow has no support elements, and its length is not restricted. There is, however, a lack of experiments on the vibrational behaviour of cylinders moving in the axial direction.

In core-annular flow, on the other hand, the models are set up for an axially moving core. Effects in thread-annular flow, like cork screw-like thread movements, could more accurately be explained by such models. As in core-annular flow wall contact may also be inhibited in thread-annular flow by irregularities of the core surface.

2. Experimental set-up and procedures

The experimental investigations on thread-annular flow were separated into two series. In the first series of experiments, mass flow, friction factor, and axial thread force were of central interest; the focus of the second series of experiments was on lateral deviations of the thread. The set-up used for the experimental determination of these values is shown in figure 2. The thread was stored on a spool that was placed inside a pressure chamber. A defined thread speed was obtained by a four-quadrant controlled electrical motor which unwound the thread from the spool. The thread was then led by rolls along a rectangular pathway over a bending beam with a resistance strain gauge, and then vertically entered the pipe 5 mm below the surface of the water. Friction forces originating from the leading rolls did not influence the recorded axial thread forces with this set-up. After the fluid and thread had passed through the pipe,

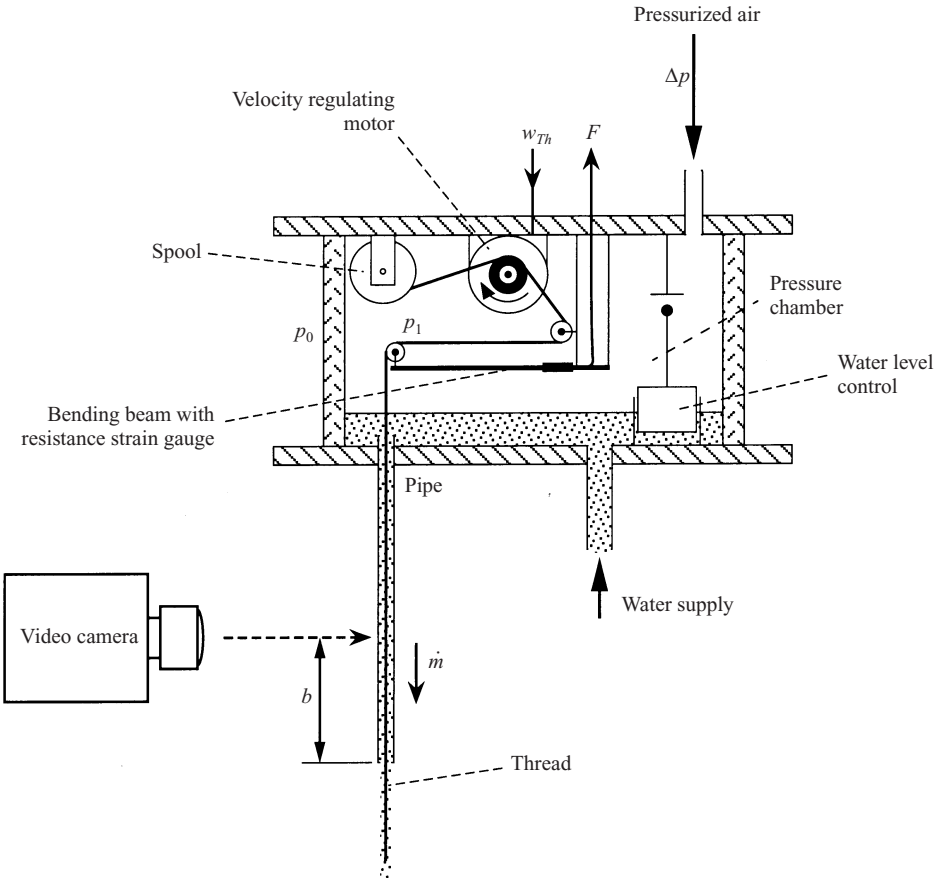

FIGURE 2. Experimental set-up for the thread-annular flow measurements. The transport of the thread from the pressure chamber through the pipe to the exit is driven by the difference between the internal (p_1) and external pressure (p_0). The thread velocity w_{Th} is controlled by the motor speed. A beam with two resistance strain gauges records the axial force F acting on the thread. The mass flow $\dot{m}$ is measured at the exit of the pipe. The optical axis of the camera was focused on the pipe perpendicular to the pipe axis and $b = 6$ cm from the pipe exit.

both were collected at the exit in a measuring cup. A video camera was used for the optical measurement of the lateral thread deviation in the glass pipe.

The experimental thread was a natural rubber monofilament with a diameter of 0.46 mm, a well-defined smooth surface and a circular cross-section. The Young's modulus of the thread was $0.69\,\mathrm{N\,mm^{-2}}$, and its bending stiffness $2.56\,\mathrm{mN\,mm^2}$. The density was $1.06\,\mathrm{g\,cm^{-3}}$, corresponding to a linear density of $0.174\,\mathrm{g\,m^{-1}}$. The transport fluid was water at a temperature of 20 °C (density $0.998\,\mathrm{g\,cm^{-3}}$, viscosity 0.001 Pa s). For the flow investigations the pipes were made of CrNi steel with parametric variations of the inner diameter between 0.55 and 1.35 mm. For the optical characterization of thread oscillations within the pipe a glass pipe with an inner diamete of 1.2 mm was used. All pipe samples had a length of 143.5 mm.

Further parameters controlling the thread-annular flow were the thread speed and the pressure inside the pressure chamber for which the experimental ranges are listed in table 1.

Parameter	Series I	Series II a	Series II b	Precision
Pressure difference	0.02–2.50 bar	0.02–2.50 bar	0.10, 0.30, 0.50 bar	±0.01 bar
Thread velocity	0–1.5 m s^{-1}	0	0.1–1.1 m s^{-1}	±5%
Inner pipe diameter	0.55–1.35 mm	1.20 mm	1.20 mm	±0.02 mm

TABLE 1. Experimental range of the varied parameters. In series I, friction factor and axial thread force were investigated; in series II, lateral deviations of the thread were measured. The last column indicates the estimated error.

Series I: Measurement of axial thread force and mass flow

The axial thread force was determined by two resistance strain gauges on the bending beam. Calibration was achieved by attaching standard weights to the thread at the pipe exit. The mass flow of the water was determined by measuring after each experimental run the mass of ejected water and thread and the thread length. The thread speed resulted from the measured length divided by the time of the experimental run.

In this set-up, particular consideration had to be given to the fact that an axial force acting on the rubber thread resulted in a longitudinal extension and a lateral contraction. The original thread radius at zero load therefore had to be corrected. The rubber thread was assumed an incompressible solid allowing Poissons's ratio to be set to 0.5 (Gauthier 1995). When Hooke's law is applied, the difference to the thread radius r_{Th} of the unloaded state can be written as

$$\Delta r_{Th} = -0.5\, r_{Th}\, \frac{F}{EA}. \tag{1}$$

F is the longitudinal force, A the cross-sectional area of the unloaded thread and E the Young's modulus. This equation is only valid if F acts at the end of the thread. If entrance and exit effects are neglected, it can be assumed that the axial force linearly decreases to zero from the measured force at the pipe entrance to the pipe exit. The diameter of the thread thus increases from the pipe entrance towards the exit. Equation (1) can therefore only be applied at the pipe entrance, where F is the measured axial force. To simplify matters we used a mean $\overline{\Delta r_{Th}}$ corresponding to the mean thread force:

$$\overline{\Delta r_{Th}} = 0.5\, \Delta r_{Th}. \tag{2}$$

Introducing the experimental values for the thread, the thread radius corrected by $\overline{\Delta r_{Th}}$ was found to be

$$r_{Th,Corr} = r_{Th} - (F \times 0.46\ [\mathrm{mm\,N^{-1}}]). \tag{3}$$

This force-adjusted geometry of the annular gap was taken into account in the evaluation of the measured data. the flow values presented below, however, always refer to the radius ratio of the undeformed thread.

Moreover, due to continuity the mass flow of the thread must be constant in any section of the pipe:

$$w_{Th} A = \text{const.} \tag{4}$$

Since the thread diameter is increased along the pipe, the thread velocity is higher at the entrance than at the exit. To calculate the theoretical thread force and friction factor a mean thread velocity is defined at the corrected thread radius $r_{Th,Corr}$,

expressed in terms of the thread velocity determined in the experiments:

$$\overline{w_{Th}} = w_{Th,\exp}\left(1 - 0.25\frac{F}{EA}\right)^{-2}. \tag{5}$$

Besides the correction due to thread elasticity the thread force must further be corrected, because the thread section between the pipe exit and the measuring cup and the fluid flowing on that thread surface cause another force component in addition to the thread-annular force in the pipe. This correction term was determined for $w_{Th} = 0$ by measuring the force difference between the situation when the thread was hanging out of the pipe into the measuring cup, and when the thread was cut off at the pipe exit. This difference was subtracted from the measured forces; this was also done for positive thread velocities $w_{Th} > 0$.

Series II: Measurement of lateral thread motions

During the second experimental series the lateral deviation of the thread from the concentric position was measured. Furthermore, the mass flow of water was determined to evaluate the flow regime in terms of the Reynolds number.

The thread position was optically recorded by a video camera (Kappa, CF 100x, figure 2). On an individual 50 Hz image (figure 3) ten equal horizontal image stripes of the vertical thread silhouette inside the pipe were recorded. The image stripes all recorded the same image section of the pipe with a constant delay of 1/500 s. As such a 500 Hz image only corresponded to a vertical pipe section of 0.13 mm, only horizontal shifts in thread position could be investigated (figure 3*c*).

An image processing program (RSB 1996) was used, and the position of the thread centre was determined for a time interval of 1 s. The result was the distance d between thread centre and pipe centre in orthogonal projection (figure 3*b*). The experimental error was estimated to be 0.01 mm. Statistical evaluation and vibrational analysis of the thread position data was carried out with mathematical software (Mathematica™, Matlab™).

3. Model of the concentric thread-annular flow

In a first approximation, the laminar thread-annular flow is described as a solid circular concentric cylinder in pipe flow (figure 4). The fluid is assumed to be incompressible and Newtonian. A similar approach was presented by Koch & Feind (1958). Influences of the pipe entrance and the exit as well as gravity and buoyancy are neglected. The velocity of the thread is used as a constant parameter.

For a fully developed and axisymmetrical steady-state flow, the Navier–Stokes equation can be reduced to

$$\frac{\partial p}{\partial r} = 0, \tag{6}$$

$$\mu\frac{1}{r}\frac{\partial}{\partial r}\left(r\frac{\partial w_z}{\partial r}\right) - \frac{\partial p}{\partial z} = 0 \tag{7}$$

where r is the radial direction; w_z is the fluid velocity, and $\partial p/\partial z$ the pressure gradient, both in the z-direction along the pipe axis. In an axially uniform gap $\partial p/\partial z$ is constant. In the following, the subscript z is omitted. Th and P designate thread and pipe. The boundary conditions of the velocities at the thread surface and at the pipe wall are

$$w(r_{Th}) = w_{Th}, \quad w(r_P) = 0. \tag{8}$$

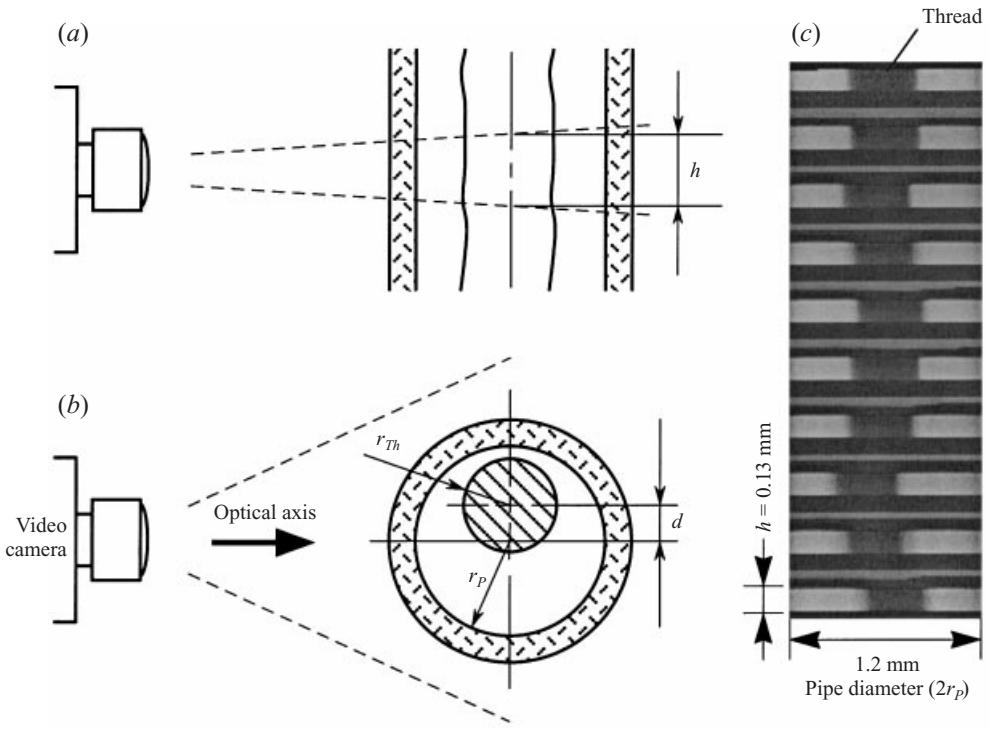

FIGURE 3. Optical recording of the thread position in the vertical pipe seen from the side (*a*) and from above (*b*). (*a*) The height of a single image was $h = 0.13$ mm which allowed the extraction of only information about lateral deviation. (*b*) The distance d between thread and pipe centre was obtained by image analysis. r_{Th} is the radius of thread, r_P the radius of the pipe. (*c*) Video image with ten picture stripes of a section of the pipe with a time delay of 1/500 s. The lateral image borders correspond to the pipe wall. In the centre the dark thread contours are seen.

To simplify the solution, the equations are transformed into dimensionless form by

$$\hat{r} = r/r_P, \quad \hat{z} = z/r_P \tag{9}$$

$$\hat{w} = w r_P \rho/\mu. \tag{10}$$

The introduction of the kinematic viscosity $\nu = \mu/\rho$ yields for the thread-annular flow the dimensionless parameters:

radius ratio

$$\xi = r_{Th}/r_P, \tag{11}$$

pressure gradient

$$\hat{P} = -\frac{\partial p}{\partial z}\frac{r_P^3}{\nu^2\rho}, \tag{12}$$

shear stresses for a Newtonian fluid

$$\hat{\tau} = \tau\frac{r_P^2}{\rho\nu^2}, \tag{13}$$

forces

$$\hat{F} = \frac{F}{\rho\nu^2}. \tag{14}$$

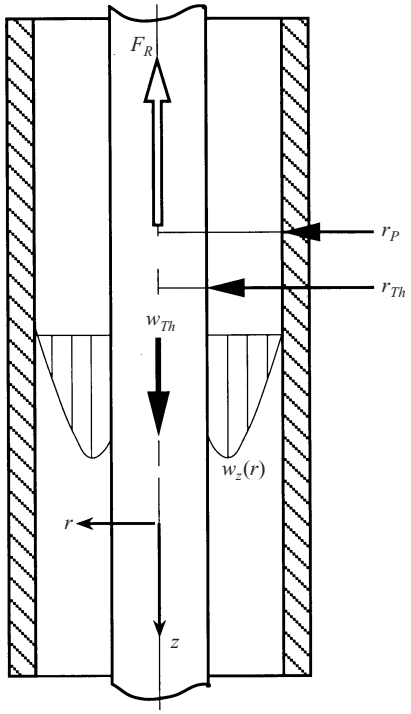

FIGURE 4. Schematic model of the thread-annular flow: the thread is assumed to be a concentric cylinder with radius r_{Th} and a constant velocity w_{Th}. A resistance force F_R (in practice deriving from the spool) is acting in the opposite direction to the thread motion. z and r represent the axial and the radial coordinates.

Equation (7) can be rewritten

$$\frac{1}{\hat{r}}\frac{\partial}{\partial \hat{r}}\left(\hat{r}\frac{\partial}{\partial \hat{r}}\hat{w}(\hat{r})\right) + \hat{P} = 0. \tag{15}$$

The dimensionless boundary conditions of equation (8) lead to the radial velocity profile:

$$\hat{w}(\hat{r}) = \tfrac{1}{4}\hat{P}\left(\hat{r}^2 + \frac{\ln \hat{r}}{\ln \xi}(1-\xi^2) - 1\right) + \frac{\ln \hat{r}}{\ln \xi}\hat{w}_{Th}. \tag{16}$$

In the pipe flow there are different forces which affect the thread in the axial direction. The shear force $\hat{F}_\tau$ results from the shear stress $\hat{\tau}_{Th}$ acting on the thread surface:

$$\hat{F}_\tau = 2\pi\xi\hat{l}\hat{\tau}_{Th}, \tag{17}$$

where $\hat{l}$ is the thread length in the pipe flow. The normalized axial shear stress for a Newtonian fluid is equal to the radial velocity gradient of equation (16).

A pressure force $\hat{F}_P$ arises from the pressure gradient along the pipe which is acting in the axial direction on the cross-section of the thread. It is equivalent to the buoyancy force acting on a body in a still fluid with a free surface, as in such a fluid column there is an analogous pressure gradient in the vertical direction. The pressure force can be written for a constant pressure gradient $\hat{P}$ in terms of the total pressure difference $\Delta\hat{p} = \hat{P}\hat{l}$ over the thread length:

$$\hat{F}_P = \pi\xi^2\Delta\hat{p}. \tag{18}$$

In steady-state flow, the shear and pressure forces $\hat{F}_\tau$ and $\hat{F}_P$ are assumed to be the only fluid-dynamic forces acting in the axial direction on the thread section inside the pipe flow. They must be in equilibrium with the resistance force $\hat{F}_R$ derived in the actual thread injection process from the spool or a similar thread package:

$$\hat{F}_R = \hat{F}_\tau + \hat{F}_P, \tag{19}$$

which can explicitly be expressed as

$$\hat{F}_R = \Delta\hat{p}\frac{\pi}{2}\frac{1-\xi^2}{|\ln\xi|} - 2\pi\hat{l}\frac{\hat{w}_{Th}}{|\ln\xi|}. \tag{20}$$

The axial force measured in the experiments presented corresponds to $\hat{F}_R$, because all the parameters in equation (20) including the thread velocity are given. All influences from the spool are thus taken into account by setting these parameters.

The total axial thread force diminishes with increasing thread velocities, because the shear force component becomes negative. At a specific thread velocity the negative shear force is equal to the pressure force, and the total thread force is zero. In practice, a thread would only move through the pipe at this velocity if there were no resistance force. This thread velocity is designated as the maximum theoretically achievable thread velocity $\hat{w}_{Th,max}$ in thread injection. It is obtained by setting the left-hand side of equation (20) to zero:

$$\hat{w}_{Th,max} = \frac{\Delta\hat{p}}{\hat{l}}\frac{1-\xi^2}{4}. \tag{21}$$

The volumetric flow rate of the concentric thread-annular flow $\hat{Q}$ is obtained by integrating equation (16) over the annular cross-section. By using dimensionless values the Reynolds number, usually expressed by the mean velocity $\bar{w}$, can be transformed to

$$Re = \frac{\bar{w}d_H}{\nu} = \frac{2\hat{Q}}{\pi(1+\xi)}, \tag{22}$$

where the hydraulic diameter for a circular annular flow is $d_H = 2(r_P - r_{Th})$. The friction factor λ is used in the same way as in the studies of Koch & Feind (1958):

$$\Delta p = -\lambda\rho\frac{l}{d_H}\frac{\bar{w}^2}{2} \tag{23}$$

and in dimensionless quantities:

$$\lambda = -\hat{P}\frac{4(1-\gamma)}{(\hat{Q}/\pi(1-\gamma^2))^2}. \tag{24}$$

If equation (22) is used, the friction factor of the thread-annular flow can be written in terms of the Reynolds number:

$$\lambda = k64/Re. \tag{25}$$

This expression differs from the pipe flow by a factor k for thread-annular flow:

$$k = \frac{(1-\xi)^2\ln\xi(\hat{w}_{Th}(1-\xi^2+2\xi^2\ln\xi)+Re(1+\xi))}{((1+\xi^2)\ln\xi+1-\xi^2)Re(1+\xi)}. \tag{26}$$

For the turbulent flow regime, empirical correlations are used in these preliminary studies to estimate mass flow and friction factor. Turbulent velocity profiles may be the subject of future investigations where the work of Huang, Christodoulou & Joseph

(1994) may be applied. In our experiments, the flow was assumed to be hydraulically smooth so that the Blasius equation can be used for $Re < 10^5$ to approximate the friction factor:

$$\lambda = (100Re)^{-1/4}. \tag{27}$$

The experimental friction factor was obtained by evaluating equation (23). This enabled a comparison with equation (25) for the laminar flow; in the turbulent case, however, the comparison with equation (27) is only possible for the axially non-moving thread.

3.1. *Statistical investigations and vibration analysis of lateral thread deviation*

For the evaluation of the acquired data, the thread deviation d from concentricity (figure 3*b*) was related to the dimensions of the annular gap by introducing a dimensionless eccentricity:

$$x = d/(r_P - r_{Th}). \tag{28}$$

For the concentric case it is zero. If the thread touches the pipe wall it corresponds to unity. For a first statistical analysis, the thread's mean deviation over time from the concentric position was calculated:

$$\bar{x} = \lim_{T\to\infty} \frac{1}{T} \int_{-T/2}^{T/2} |x(t)|\, \mathrm{d}t, \tag{29}$$

which is equivalent to the mean eccentricity. T is the examined time interval. As T cannot be infinite in the experiments, the thread vibrations are assumed to be an ergodic process where they are stationary and independent of time history $x(t)$ (Meirovitch 1986).

To distinguish smooth waves or even constant values from very peaky oscillations, axial symmetry of eventual thread vibrations was investigated by calculating the probability density function, which is defined as:

$$p_{stat}(x) = \lim_{\Delta x\to 0} \frac{P_{stat}(x+\Delta x) - P_{stat}(x)}{\Delta x} = \frac{\mathrm{d}P_{stat}(x)}{\mathrm{d}x}. \tag{30}$$

$P_{stat}(x)$ is the probability of the thread being closer than x to the pipe centre. The index *stat* is used to distinguish this statistical value from the pressure symbol. The statistical distribution $p_{stat}(x)$ of the thread position over the pipe diameter may additionally be used to extract information about the thread movement in the direction of the optical axis perpendicular to the image plane. This is possible because different forms of thread motion in the plane that is perpendicular to the pipe axis, such as circular or star-shaped movements, deliver different probability density distributions.

The third point that is of interest in thread vibration analysis involves dominant frequencies. Therefore, the power spectrum $S_x(\omega)$ was calculated, still assuming an ergodic process:

$$S_x(\omega) = \int_{-\infty}^{\infty} R_x(\tau)\, \mathrm{e}^{\mathrm{i}\omega\tau} \mathrm{d}\tau \tag{31}$$

where $R_x(\tau)$ is the autocorrelation function of the time delay τ given by

$$R_x(\tau) = \frac{1}{T} \int_{-T/2}^{T/2} x(t)\, x(t+\tau)\, \mathrm{d}t. \tag{32}$$

The scanning theorem of Shannon (Geering 1990) states that only frequencies of

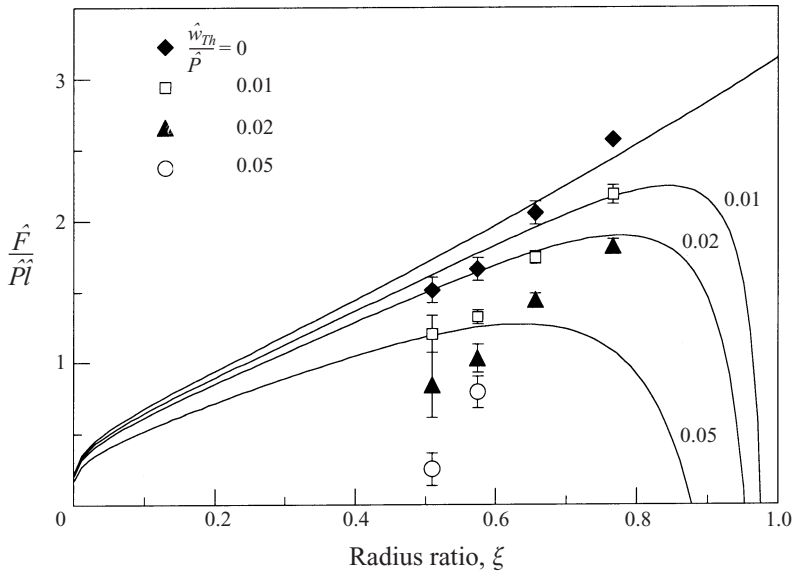

FIGURE 5. Dependence of normalized axial thread force $\hat{F}/(\hat{P}\hat{l})$ on the radius ratio ξ ($Re \approx 100$). A marked increase is observed with increasing ξ. For low ξ the measurements (symbols) show lower values than the laminar concentric theory (curves): at higher ξ they exceed the theoretical curve. Thread velocity has a decreasing effect on the thread force, which is much more pronounced in the experiments than predicted by laminar concentric theory.

Pipe diameter [mm]	0.6	0.7	0.8	0.9
Pressure difference [bar]	1.0	0.50	0.20	0.16
Thread force [mN] for $\hat{w}_{Th}/\hat{P} = 0$	23.9	13.8	6.97	7.01
$\hat{w}_{Th}/\hat{P} = 0.01$	20.4	11.9	5.88	6.01
$\hat{w}_{Th}/\hat{P} = 0.02$	17.2	8.63	4.96	4.84
$\hat{w}_{Th}/\hat{P} = 0.05$	—	—	4.19	2.93
Force correction [mN] for $\hat{w}_{Th}/\hat{P} = 0$	0.78	1.22	1.66	2.12

TABLE 2. Mean values of the uncorrected measured axial thread forces and the correction term with which the thread forces shown in figure 5 are obtained.

up to half of the recording frequency are relevant. Frequencies above 250 Hz were therefore neglected in our investigations.

4. Results and discussion

4.1. *Axial forces acting on the thread*

The measured and corrected data on the axial thread forces were transformed to dimensionless values and normalized by the pressure difference $\hat{P}$ and the pipe length $\hat{l}$. In figure 5 the results for different radius ratios and pressure-normalized thread velocities are presented along with the theoretical solutions of equation (20). The measurements were conducted in the low laminar range, around Reynolds numbers of $Re = 100$.

For all thread velocities the thread force increases with the radius ratio in figure 5. On the other hand, the axial thread force decreases with a rise in the thread velocity.

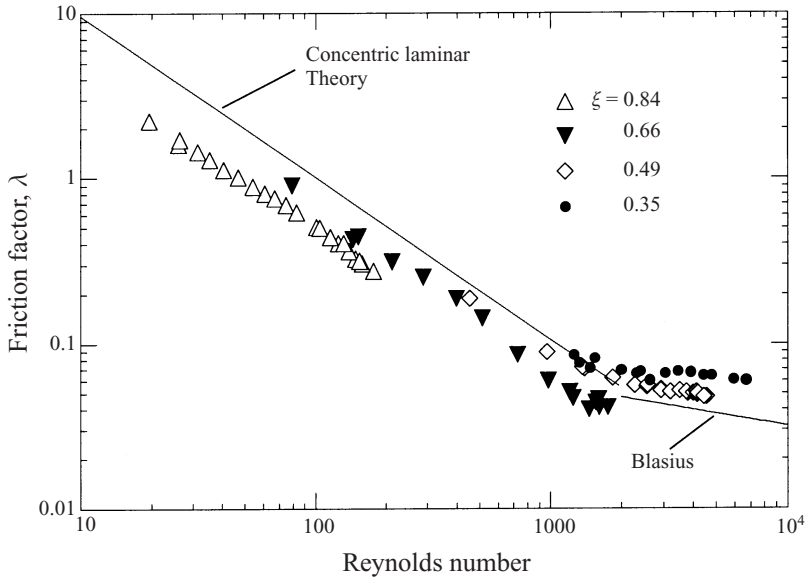

FIGURE 6. Friction factor vs. Reynolds number at different radius ratios ξ and thread velocity $w_{Th} = 0$. In narrow annular gaps thread eccentricity could be the reason for the lower measurements in the laminar range. For wide annular gaps the high experimental values compared to Blasius exist because the empirical correlation of Blasius is set up for pure pipe flow.

Experimental values show a much more pronounced decline with an increase of thread velocity than the laminar theory. In particular, this discrepancy becomes larger with the width of the annular flow gap, for low values of radius ratios. The description of the axial thread force in annular pipe flow that the laminar concentric model delivers is therefore only sufficiently accurate for an axially non-moving thread. For a moving thread the deviations from theory may arise from the eccentric thread position and possible secondary lateral flow, as assumed by Eifler & Nijsing (1971) in eccentric annular flow, but unsteady lateral movements of the thread could also affect the axial thread force.

In addition, the substantial deviation from theory for positive thread velocities may be caused by corrections due to the thread section hanging out of the pipe being too large. For the axially moving thread the correction terms are expected to be smaller than the ones listed in table 2 for $w_{Th} = 0$. The measurements would probably be more in line with the theory if in future work the correction term could also accurately be determined for $w_{Th} > 0$.

Even at the highest thread velocities, however, analogous to the model, the experiments show an increase of the thread force with radius ratio; this parameter can therefore be considered an essential factor that affects the axial thread force.

4.2. *Friction factor of thread-annular flow with axially non-moving thread*

Figure 6 shows the theoretical friction factor for the laminar and turbulent concentric annular flow for different radius ratios. The theoretical curves are compared to the experimental friction factors resulting from the measured mass flow by equation (23). The thread was axially fixed at the upstream end in this experimental series, so $w_{Th} = 0$.

At radius ratios close to unity ($\xi = 0.84$) only data from the laminar range could

be investigated, while in the case of wide annular gaps ($\xi = 0.35$) mainly data for the transition range and the turbulent flow range were obtained. This restriction was due to the fact that in our experimental set-up the reading accuracy of the manometer decreased near zero and the maximum pressure difference was limited to 2.5 bar.

The transition range where the laminar flow starts to become turbulent can be estimated in figure 6 to be around $Re = 2000$ which is lower than in pipe flows with fixed cores (Koch & Feind 1958) or in core-annular flow (Arney *et al.* 1993). In our experiments we did not observe any marked transition range as in the pipe flow. As Koch & Feind (1958) assumed for rigid cores, the thread probably also has a damping effect on early turbulent disturbances; therefore the smooth change to turbulence could occur.

In figure 6 the curves of the theoretical friction factor of concentric annular flow (equation (25)) are represented by a single line, because the differences for the radius ratios in this plot are negligible. In the laminar range the experimental values are significantly smaller than theoretically assumed. This effect is more pronounced for small annular gaps such as $\xi = 0.84$. The laminar model of Shigechi *et al.* (1994) shows a corresponding decrease of the friction factor with eccentricity. In our optical investigations in § 4.4 we observed a mean eccentric position of the thread over time; we assume that this is the reason why in the experiments the friction factor was lower and the flow rate higher than in the concentric flow model.

An increase of the friction factor with decreasing radius ratio is also found in the turbulent range. In contrast to the laminar case, however, the measured values exceed the ones calculated by the empirical solution of Blasius (equation (27)), which is in line with the experiments of Koch & Feind (1958). This discrepancy is due to the fact that the Blasius equation does not contain any correction for the annular flow and only represents an empirical solution for the circular pipe flow.

The tendency of the turbulent friction factor to decrease with a decreasing annular gap nevertheless indicates that in this flow regime eccentricity could still influence the annular flow. There is a slight decrease in the friction factor at $\xi = 0.49$, and at $\xi = 0.66$ the few turbulent data points of the friction factor are even below the Blasius solution. This could indicate that eccentricity prevails over turbulent disturbance and roughness effects on the thread surface. Further, these disturbances could be damped by the wall in narrow annular gaps. This conjecture is supported by the work of Ooms (1972), where the pipe wall was found to have a reducing effect on certain instabilities of core-annular flow.

4.3. *Laminar friction factor of thread-annular flow with an axially moving thread*

The laminar friction factor of thread-annular flow with a thread moving in the axial direction was investigated for two radius ratios. A constant ratio between the experimental thread velocity w_{Th} and the maximum theoretical thread injection velocity $w_{Th,max}$ (equation (21)) was chosen which resulted from the largest possible thread velocity in the experiments.

In figure 7 the friction factor curve for an axially non-moving concentric thread can again be represented by a single line for both radius ratios. On the other hand, both theoretically and experimentally an axial thread motion results in a decrease of friction factor which at comparable velocities around $w_{Th} = 0.25\, w_{Th,max}$ shows a significant dependence on the radius ratio. In thread-annular flow with large radius ratios the fluid is mainly withdrawn by the relatively large thread surface so that Couette flow prevails. In such cases the thread velocity has a stronger reducing effect on friction factor than at lower radius ratios where pressure-controlled Poiseuille flow

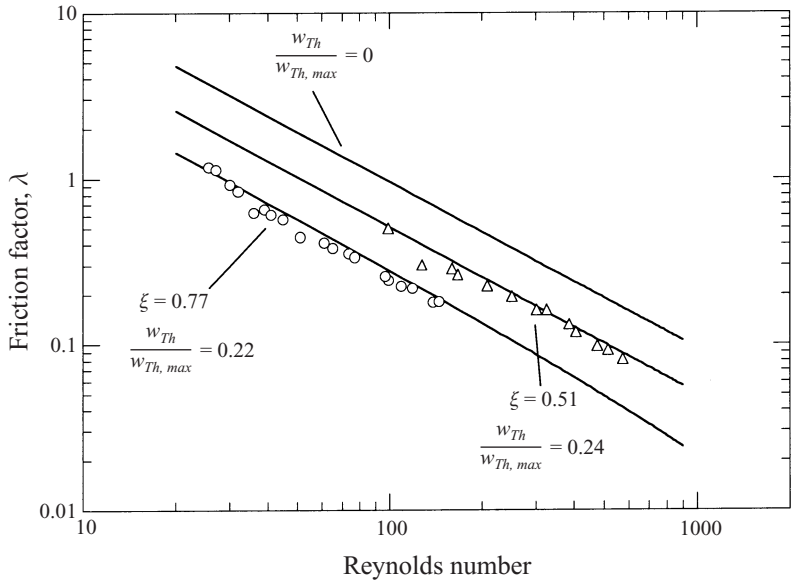

FIGURE 7. Friction factor of thread-annular flow with axially moving thread. A significant decrease is observed with thread velocity, which is more pronounced at large radius ratios ξ. The agreement of experiments with concentric laminar theory is better than for threads without axial velocity (figure 6).

is dominant in the annular gap. The agreement of the experiments with the laminar concentric theory is better than for thread-annular flow with an axially non-moving thread. For annular flow with axial thread velocity, however, the experimental values are also below the theoretical curve, which could again be an indication of an eccentric position of the thread inside the pipe. The bending tendency of the friction factor curve at $\xi = 0.77$ is a result of the correction of the thread velocity due to thread elasticity.

4.4. *Vibration behaviour of the thread in vertical pipe flow*

In some experiments with CrNi steel pipes there were strong thread vibrations at the pipe exit. Investigations in which glass pipes were used revealed that these vibrations also occur further upstream in the pipe. At the pipe entrance, however, the thread showed no significant lateral movements. The oscillations of the thread seemed to be established only 2–3 cm from the pipe entrance. Pronounced corkscrew waves as described by Bai *et al.* (1992) could not be discerned on our photographs. We noticed, however, that the thread was not completely straightened by the water flow in the annulus: figure 8(*b*) shows slight buckling and waves along the thread.

Despite these vibrations, we never observed the thread touch the pipe wall during the evaluation of the video pictures (figure 3*c*). Contact friction between the thread and the pipe wall can therefore be neglected for vertical thread-annular flow. The findings of Secomb & El-Kareh (1994) may be an explanation for the limited lateral thread deviations: they found that the resistance force to lateral motion was bigger the closer the cylinder was to the pipe wall. Additionally, in the case of eccentricity, pressure differences could occur over the circumference of the annular gap (Piercy *et al.* 1933) which could also counterbalance radial deviation. On the other hand Christopherson & Naylor (1955) found that the equilibrium position for an axially

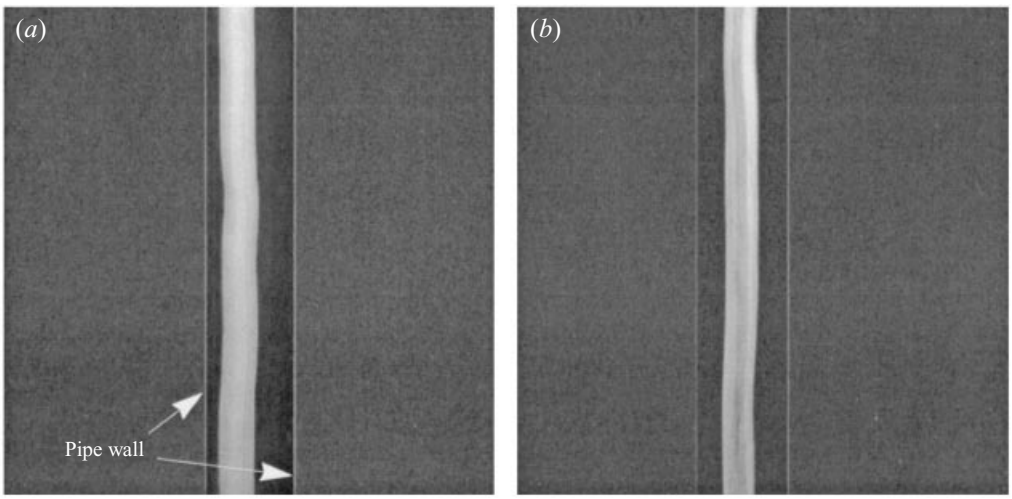

FIGURE 8. Photographs of a monofil rubber thread with circular cross-section in downstream pipe flow. (*a*) Thread in a pipe without axial velocity and fluid flow ($Re = 0$, $w_{Th} = 0\,\mathrm{m\,s^{-1}}$). The thread is not completely straight. (*b*) $Re = 2310$, $w_{Th} = 0.3\,\mathrm{m\,s^{-1}}$: The thread was never observed to touch the pipe wall, but slight buckling and waves can be recognized along the thread despite axial stretching forces which reduce the diameter. Concentricity seems to prevail.

moving cylinder in a pipe was not concentric, but eccentric. If, however, eccentricity were assumed for the stable case, the position of the thread could be located anywhere on a circular orbit of stability around the pipe centre, and thread motions on this pathway would also be stable. The transient travelling spiral waves noted by Bai *et al.* (1992) may be interpreted as such a stable core rotation around the pipe axis. This may serve as a model for the thread motion, and its validity is discussed in the sections below.

4.4.1. *Mean deviation of thread vibrations*

The influence of flow regime and thread velocity on the time-mean eccentricity is shown in figure 9 by the mean deviation of the thread position. All points correspond to single measurements of 1 s.

Figure 9(*a*) where thread velocity was zero shows that the thread has a mean eccentric position. Our assumption that eccentricity could substantially affect the thread-annular flow is therefore reinforced. The mean thread deviation shows a marked maximum at about $Re = 2700$. This may be an effect of the transition from laminar to turbulent flow. At higher Reynolds numbers $\bar{x}$ decreases again. The maximum may exist because of large temporary thread deviations caused by eddies and disturbances which in the transition range only sporadically appear in locally restricted sections of the thread circumference. At higher flow rates the intermittence factor of laminar and turbulent flow increases (Schlichting & Gersten 1997) so that more frequent disturbances may counterbalance each other over the thread circumference and result in reduced lateral thread deviations. In highly turbulent flow, where excitation by near-field noise was assumed, Chen & Wambsganss (1972) conducted experiments in a comparable range of radius ratio. On increasing the Reynolds number, rods with both ends fixed exhibited a first maximum in lateral displacement; later, with larger flow velocities, the deviations continuously rose.

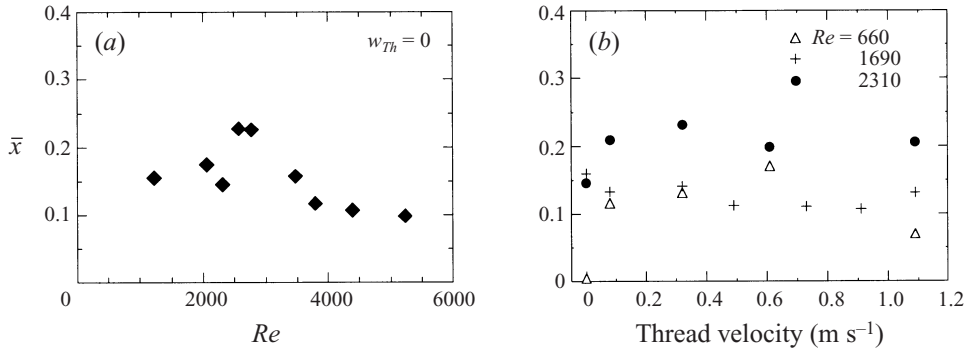

FIGURE 9. Mean eccentric position $\bar{x}$ of the thread at a radius of $\xi = 0.46$. (*a*) With increasing Reynolds number, in the transition range around $Re = 2700$, $\bar{x}$ reaches a maximum and then decreases in the turbulent flow. (*b*) No marked influence of the thread velocity on $\bar{x}$ is observed, regardless of the Reynolds number.

Mean deplacements of rods fixed only at their upstream end, however, continuously increased with the flow velocity. Whether in the highly turbulent range a similar behaviour exists in thread-annular flow has to be investigated in future experiments.

In figure 9(*b*) the thread velocity shows no significant influence on the mean deviation of the thread position. However, at $Re = 660$ the low mean thread deviation $\bar{x}$ for $w_{Th} = 0$ could result from the low axial thread forces in this flow range so that the thread behaves practically like a rigid not a vibrating body in the pipe.

4.4.2. *Probability density function of thread vibrations of an axially immobile thread*

The distributions of the probability density shown in figure 10 were calculated from data of experiments with the axially fixed thread. The plots generally have a symmetric shape which indicates that the thread has no stationary position in the pipe. At $Re = 2570$ the probability density function is distributed in the widest amplitude range around the concentric position which may again be an effect of the transition from laminar to turbulent flow. In the image plane of the recording large thread deviations almost seem to have the same probability density as small oscillations around the pipe axis. At larger or smaller Reynolds numbers the probability density plots become more narrow. Especially in the fully turbulent flow regime at $Re = 4390$, the thread increasingly seems to be kept in a concentric position which confirms the assumption that turbulent flow helps maintain a centred thread position.

Since these data also contain information about thread vibrations in the direction of the optical axis, two different models have been developed to interpret the measured data as two-dimensional movements perpendicular to the pipe axis.

First, a 'star-shaped' vibration of the thread proceeding from the concentric position was considered. Amplitudes and direction were assumed to be distributed at random, and the thread to oscillate in a sinuous form over time with constant frequency. Figure 11(*a*) illustrates a possible trajectory of such a vibrational model for the thread. This model represents lateral thread deviations from concentricity due to single flow disturbances where the thread, after reaching an eccentric position, returns to the pipe centre. Circular rotations of the thread around the pipe centre are included in a second thread motion model. It takes so-called corkscrew waves into account as they were observed by Bai *et al.* (1992) in core-annular flow. These waves moved down the pipe in a spiral way which in a plane orthogonal to the pipe axis leads to a

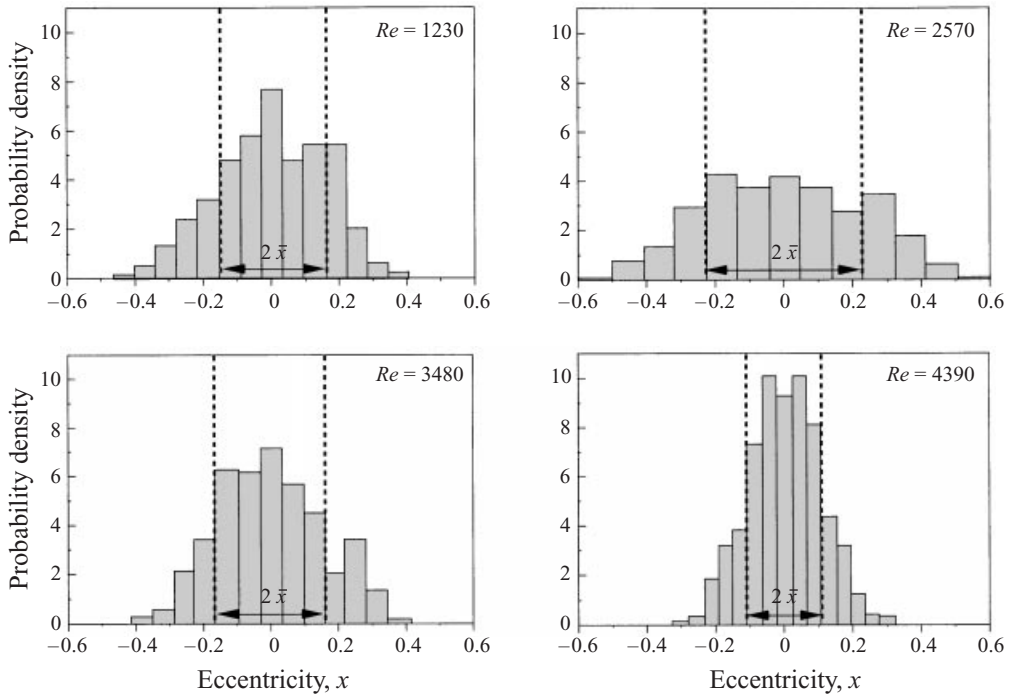

FIGURE 10. Probability density function $p_{stat}(x)$ of the lateral position of an axially fixed ($w_{Th} = 0$) thread in pipe flow. The radius ratio was $\xi = 0.46$. The distribution of the thread position is symmetric around the pipe axis. The wide distribution in the transition range at $Re = 2570$ shows that bigger thread deviations from the pipe centre appear in this range. In the turbulent flow regime the deviations decrease, as the more narrow distribution shows.

circular thread motion. In this model, the thread was assumed to rotate with constant frequency and eccentricity as shown in figure 11(*b*).

For these two models of lateral thread motion the probability density functions shown in figure 11(*c*) were calculated for the same orthogonal projection as in the experiments. The relative deviation is defined as the ratio of the thread position to an arbitrary maximal deviation. For the star-shaped motion the probability density has a sharp maximum at zero, whereas for the rotating thread the result is a saddle-shaped curve with practically constant values around the pipe centre.

Comparison of the experiments from figure 10 with the probability density of the star-shaped motion model generally shows wider and less peaky distributions. The curve for $Re = 2570$ shows nearly constant values over a wide range of deviation and a tendency to the saddle-shaped curve of a rotating thread. This may indicate that at the transition from laminar to turbulent flow the thread not only oscillates with larger amplitudes, but besides a star-shaped trajectory also has a strong orbit-like movement component. In the fully laminar and fully turbulent flow regions thread oscillations are more accurately described by the star-shape motion model.

4.4.3. *Probability density function of vibrations of a thread with axial velocity*

Figure 12 shows the probability density function of the thread position in pipe flow at different thread velocities. The pressure difference over the pipe length was constantly 0.5 bar corresponding to $Re = 2310$ for the axially non-moving thread. This pressure difference is supposed to be in the range of transition and to contain the

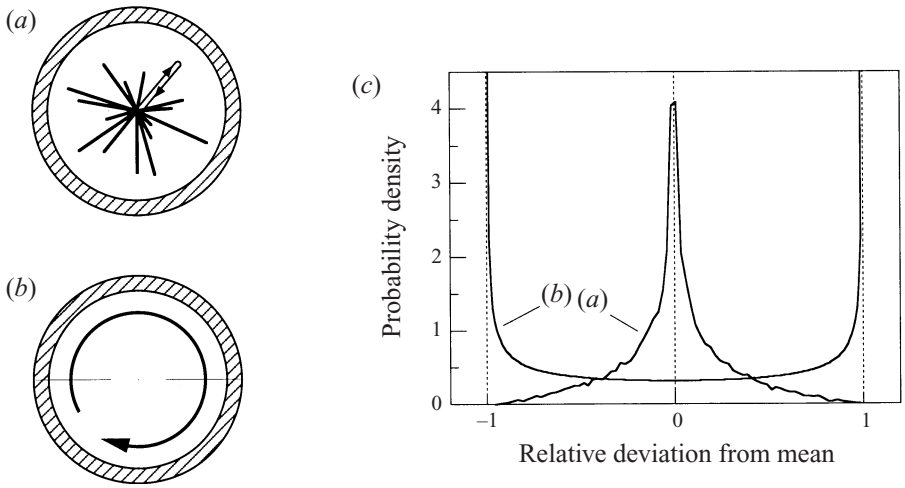

FIGURE 11. Models of lateral thread motion and their probability distributions. (*a*) Star-shaped oscillation with the pipe centre as origin. (*b*) Circular rotation of the thread around the pipe centre. (*c*) Probability density function $p_{stat}(x)$ (equation (30)) of these two models, in the same orthogonal projection of the thread position as in the experiments. The relative deviation is the ratio between the actual deviation and an arbitrary given maximum deviation.

strongest thread vibrations. Generally the probability density function resembles the distribution for the axially immobile thread at $Re = 2570$ (figure 10) where a broader distribution was observed than in the fully laminar or turbulent flow. Surprisingly, however, the probability density function is flatter at $w_{Th} = 0.32\,\mathrm{m\,s^{-1}}$ and similar to the saddle-shaped curve of a rotating thread movement. Fluid-dynamic resonance interactions between the elastic thread and the water flow may be a reason for this second thread-velocity-dependent vibrational state where the thread mostly seems to rotate on a concentric trajectory. At these thread velocities, however, no significant change in the friction factor was observed. Except for this resonance-like state the probability density function, like other investigated values, was hardly affected by the thread velocity in this range.

Apart from resonance-like states, the theoretical distribution of the random star-shaped thread motion seems to be a more accurate approximation for the probability density function of the experimental thread position than the deterministic model of the rotating thread. The probability density observed by Wambsganss & Chen (1971) for flexible cylinders which could be approximated by a normal distribution reinforces this assumption. In those experiments only vibrations in one lateral direction were possible which means that orbit-like rotations of the cylinder were inhibited. These movements could be regarded as the component of one direction of a star-shaped thread movement in thread-annular flow. Nevertheless, our data indicate rotating components superposed on the star-shaped oscillations; short tangential movements may contribute to the same effects.

4.4.4. *Frequency analysis of thread vibrations of an axially immobile thread*

Besides the position of the thread in the pipe and its distribution over time, the vibration frequencies of the thread are of interest. The influence of the Reynolds number on the vibration frequencies is shown in figure 13 by the power spectral density function $S_x(\omega)$ (equation (32)) of the radial deviation of an axially non-moving thread. The ordinate shows the relative power spectral density where for a

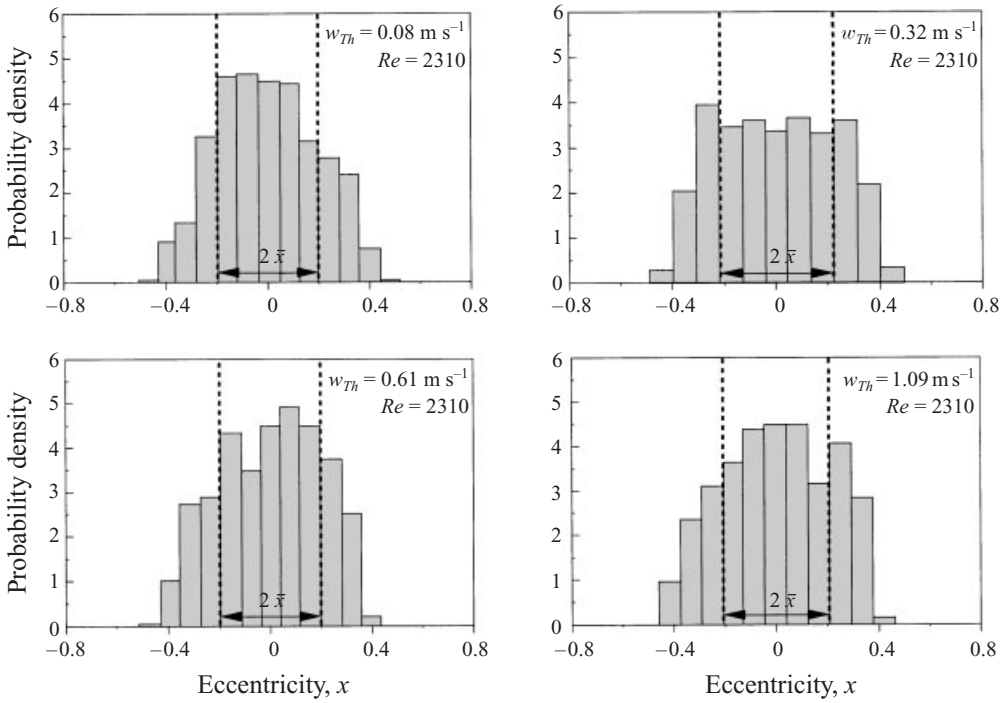

FIGURE 12. Probability density function $p_{stat}(x)$ of the thread position in pipe flow at different axial thread velocities w_{Th}. The radius ratio was $\xi = 0.46$. Generally, the thread velocity hardly affects the probability density function. A saddle-shaped distribution appears at a thread velocity of 0.32 m s^{-1} which is similar to the distribution of a thread rotating on a circular orbit (figure 11*b*).

better overview of the data the zero points were vertically shifted. The original power spectral density function was smoothed by using a convolution algorithm.

With increasing Reynolds numbers a general shift of the dominant frequencies to higher values is observed. At $Re = 2570$, i.e. in the transition range, dominant frequencies reach their maximal values with the highest peaks at 51 and 55 Hz. A resonance-like state may exist in this flow range.

In the turbulent flow regime, oscillations with large intensities are further shifted towards higher frequencies, but at the same time the intensities of the dominant frequency bands decrease. Low-turbulence flow not only seems to have a centring effect by decreasing the mean thread deviation $\bar{x}$ (Figure 9*a*), but it also inhibits thread vibrations with big amplitudes.

The resonance-like state at $Re = 2570$ may appear due to transient disturbances in the transition range which were already discussed in connection with the mean thread deviation $\bar{x}$ in figure 9. Transient disturbances could lead to single large deviations of the thread. After such a lateral excursion, the thread possibly oscillates at a damped transversal natural frequency until a new axially moving flow disturbance 'package' again stimulates the vibration. When considering the probability density function in figure 10 at the same Reynolds number $Re = 2570$, the dominant peaks around 55 Hz in the power spectral density plot could be caused by a resonance-like rotating thread motion, maybe similar to corkscrew waves in core-annular flow. In his experiments Paidoussis (1966*a*, *b*) also observed that a flexible cylinder with a free end in axial flow oscillates in a rotating plane while the free end describes a quasi-circular path.

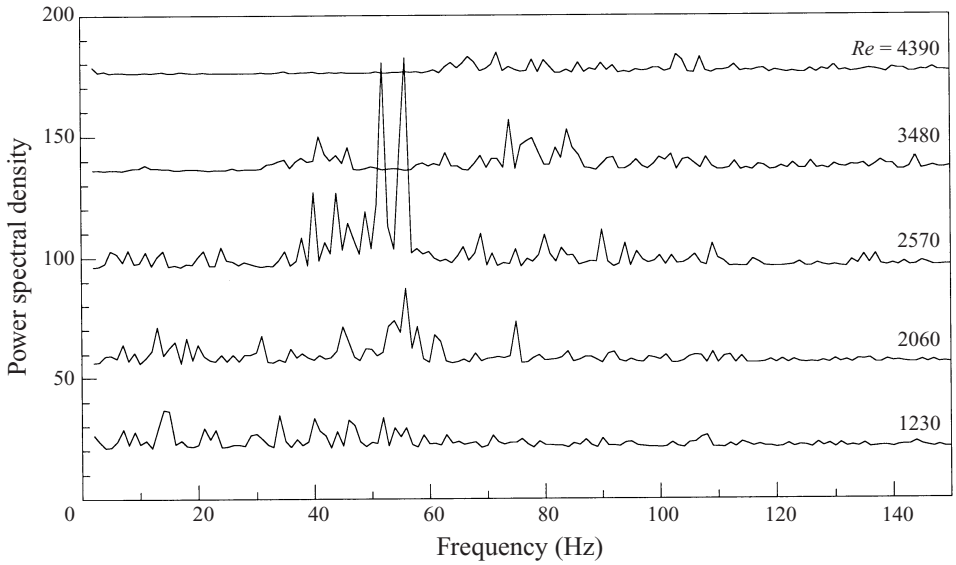

FIGURE 13. Power spectral density function of lateral thread vibrations in pipe flow at different Reynolds numbers. The thread velocity was $w_{Th} = 0$. Strong peaks appear around 55 Hz for $Re = 2570$ in the range of transition from laminar to turbulent flow. Low-frequency vibrations are attenuated in the turbulent flow.

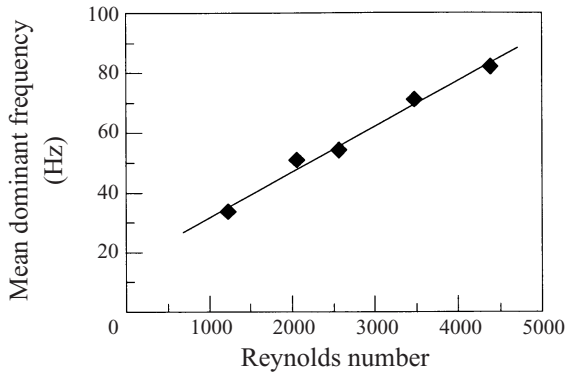

FIGURE 14. General shift of mean dominant frequencies $\bar{f}$ to higher values with the Reynolds number. A linear behaviour correlates well with the data (linear curve fitting $R = 0.99$).

The general shift of the dominant oscillations in thread-annular flow towards higher frequencies at increased fluid flow does not occur at one fundamental frequency, but it is rather a range of dominant oscillations that is shifting. An explanation may be found in the research of Paidoussis & Pettigrew (1979) on cylinders in confined axial flow; they demonstrated a continuous succession of instabilities of increasingly complex modal shape which could interfere in thread-annular flow. For a more quantitative discussion of this frequency shift the mean dominant frequencies were calculated in figure 13 for the respective Reynolds numbers. Only frequencies with intensities which were more than one third of the power spectral density maximum above the mean value were considered. Figure 14 shows a nearly linear increase of the mean dominant frequency with the Reynolds number. In similar experiments with flexible cylinders in axial flow Chen & Wambsganss (1972) found that the

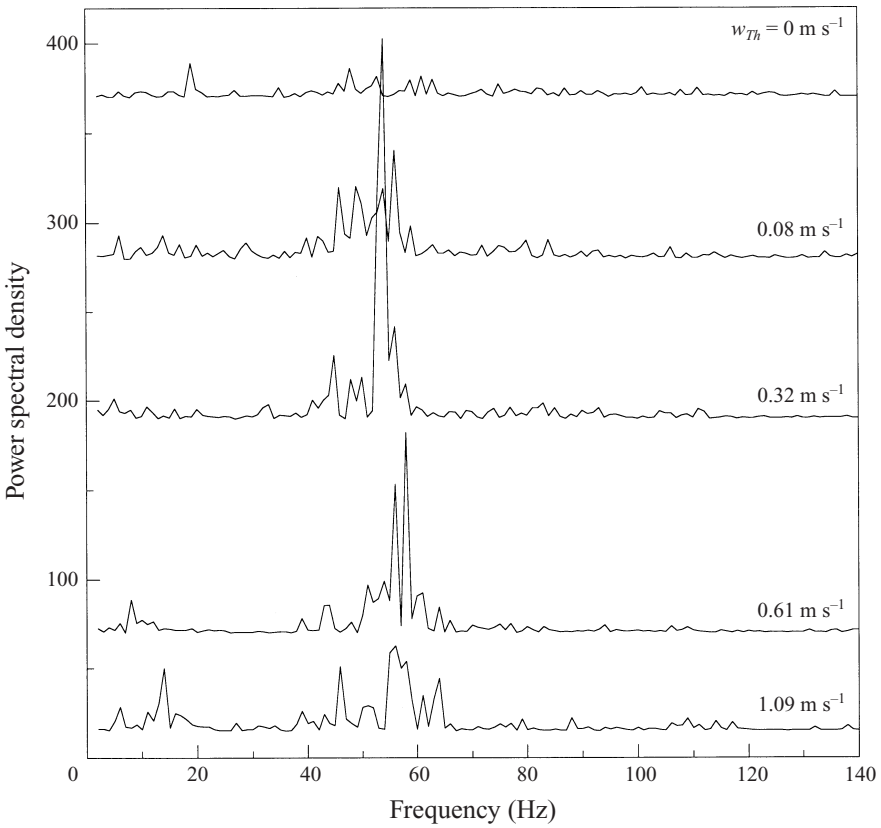

FIGURE 15. Power spectral density function of lateral thread vibrations at different axial thread velocities w_{Th} in pipe flow. At $Re = 2310$ no frequency shift of the bands is observed with changing thread velocity, but the vibrational intensity is significantly affected. A resonance-like maximal peak appears at a thread velocity of 0.32 m s^{-1}.

fundamental frequency of cantilevered rods was increasing along with the mean axial flow velocity. Rods with fixed–fixed end conditions, on the other hand, showed a decreasing behaviour of the fundamental frequency. In this respect, cantilevered rods are more comparable to a thread in pipe flow; in contrast to our investigations, however, highly turbulent flow and large hydraulic diameters were considered.

In summary, the range of dominant frequencies appears to increase with the axial fluid velocity, while the intensity of the vibrations is influenced, rather, by the flow regime.

4.4.5. *Frequency analysis of thread vibrations of a thread with axial velocity*

Figure 15 shows that the vibrational behaviour is also strongly affected by thread velocity. The corresponding Reynolds number for thread-annular flow with an axially non-moving thread was $Re = 2310$. Generally, peaks of the power spectral density are high and concentrated in narrow bands in this range, as already observed for the axially non-moving thread at $Re = 2570$ (figure 13). By varying the thread velocity a second resonance-like state is found around 55 Hz for $w_{Th} = 0.32$ m s^{-1}. The saddle-shaped probability density function found at the same thread velocity (figure 12) reinforces the assumption that the thread executes a circular motion around the pipe centre at the observed pipe section, possibly comparable to the motion of axially

moving cork-screw waves. Moreover, for a thread without axial velocity the maximum power spectral density around 55 Hz is considerably lower than for a moving thread, even compared to a small thread velocity of only $w_{Th} = 0.08\,\mathrm{m\,s^{-1}}$ (figure 15). In summary, the amplitudes were strongly affected by the thread velocity w_{Th} in this range of Reynolds number, whereas no shift of dominant frequencies was observed when this parameter was varied.

5. Conclusions and outlook

5.1. *The experimental set-up for thread-annular flow*

The experimental set-up allows measurement of axial thread force and mass flow in annular pipe flow with an axially moving core of unlimited length, like, for instance, a thread. Comparable investigations are found in cooling problems of optical fibre draw-off, but there the focus was on the determination of the temperature behaviour (Vaskopulos, Polymeropoulos & Zebib 1993). Our apparatus makes it possible to obtain fundamental flow data under isothermal conditions and could be used to discuss purely theoretical investigations on turbulent annular flow with moving cores, such as conducted by Shigechi *et al.* (1990). The set-up could be improved for future experiments in the following respects: a thread with negligible lateral contraction should be used, and higher pressure differences over the pipe length should be applied to enable measurements at Reynolds numbers in the higher turbulent flow regime.

5.2. *Experimental findings and applicability of the laminar concentric model*

The experimental investigations on thread-annular flow show an increasing axial thread force with increasing radius ratio. The axial thread velocity generally reduces the axial thread force; the measurements at low radius ratios, however, are found to be significantly lower than predicted by theory.

The friction factors derived from the mass flow measurements show a pronounced dependence on the radius ratio for an axially non-moving thread. The smaller the annular gap between pipe wall and thread, the further the friction factor lies below the predictions of laminar concentric theory. This is a strong indication that the thread-annular flow is affected by eccentricity of the thread which results from the lateral thread vibrations recorded in our optical experiments. In accordance with Redberger & Charles (1962), eccentricity had its largest influence on the flow rate at large radius ratios.

In the turbulent flow regime the measured friction factor exceeds the empirical solution of Blasius for low radius ratios, because the solution of Blasius is set up for circular pipe flow. Better agreement with the measurements could be expected by applying accurate turbulent models such as the model of Shigechi *et al.* (1990) or the k-ε model of Huang *et al.* (1994) for core-annular flow.

The thread velocity is found to have a significant decreasing effect on the thread-annular friction factor in the laminar flow range, which is in agreement with the concentric laminar model. On the other hand, deviations from theory were considerable for an axially non-moving thread which shows that the two flow types of thread-annular flow, one with an axially non-moving thread, the other with an axially moving thread, have to be regarded as different flow cases.

In general, the laminar theory yields satisfying predictions for an axially non-moving thread in annular flow. Further studies need to be conducted, however, to understand the reducing effect on the axial thread force with thread force. Eccentric-

ity, vibrations, and secondary lateral flow could be factors that have an influence on the thread force; this could, for instance, be investigated by optical means.

5.3. *Lateral thread vibrations*

Vibrational analysis of our experimental data shows that Reynolds number and thread velocity have a significant influence on the vibration behaviour of the thread: in the case of an axially non-moving thread, dominant vibrations generally shift towards higher frequencies with increasing Reynolds number. Transient flow conditions, such as eddies and disturbances, stimulate resonance-like states of the thread-annular flow system, so that the highest amplitudes and intensities are found in the transition range. In the fully turbulent range, the vibrations are more and more damped. In the case where the thread has an axial velocity in the pipe the vibrations are more intense and have larger amplitudes than in the case of the fixed thread. In the early turbulent flow regime, the thread speed has no influence on the dominant frequencies, but resonance-like maximal amplitudes appear at certain thread velocities.

The resonance-like vibrating states show an increased component of rotational thread movement, which is supposed to be associated with corkscrew wave-like thread movements inside the pipe. This could be important for the medical application of thread injection, because such thread movements may lead to a spiral-shaped deposition of the thread within the injection channel and, subsequently, to a potential blockage of the injection system as observed in preliminary experiments with radius ratios of $\xi < 0.3$. Such vibrational states should be avoided for reliable clinical thread injection applications.

Moreover, these experiments show that the thread has a mean eccentric position over time which is reduced in low-turbulence flow.

Lateral thread vibrations and eccentricity probably affect both mass flow and axial thread force, and could be the reason for discrepancies with the concentric laminar theory. On the other hand, the resonance-like vibrations were not observed to have an effect on mass flow and axial thread force and can therefore be neglected in this respect.

Future investigations on the influence of the radius radio on thread vibrations could contribute to a more thorough understanding of these effects.

5.4. *Relevance for clinical application*

For high reliability of the thread injection, large radius ratios should be chosen, because the axial thread force to overcome potential resistance is highest in this range. Lowest friction factors are also found at large radius ratios. At the same time, the fluid consumption at a constant pressure difference is the lowest in narrow annular gaps.

In our investigations, there was never any contact between the thread and the pipe wall, not even at the most intense vibrations. Contact friction between thread and pipe wall is therefore not expected to inhibit thread injection in straight pipes, and does not have to be taken into consideration for the design of medical devices.

The variations of flow conditions at the pipe exit have not been investigated in this work, although they may significantly influence the behaviours of both the fluid and the thread. In our experiments an exit into ambient air was chosen, but in medical applications fluid and tissue at the exit may significantly disturb the thread-annular flow. Further analysis and refinement of the thread-annular transport phenomena are required to optimize the performance of injection devices. In particular, the influence of the resistance force of the thread spool has to be taken into account for an optimal thread injection system.

The authors wish to thank Dr J. Mayer, K.-L. Eckert, and Dr B. Müller whose comments were helpful in the revision of the manuscript, and Th. and F. Brandsberg for their constructive support in the design of the experimental apparatus.

REFERENCES

Arney, M. S., Bai, R., Guevara, E., Joseph, D. D. & Liu, K. 1993 Friction factor and holdup studies for lubricated pipelining – I: experiments and correlations. *Intl J. Multiphase Flow* **19**, 1061–1076.

Bai, R., Chen, K. & Joseph, D. D. 1992 Lubricated pipelining: Stability of core-annular flow. Part 5. Experiments and comparison with theory. *J. Fluid Mech.* **240**, 97–132.

Bai, R., Kelkar, K. & Joseph, D. D. 1996 Direct simulation of interfacial waves in a high-viscosity-ratio and axisymmetric core-annular flow. *J. Fluid Mech.* **327**, 1–34.

Chen, S. S. 1987 *Flow-induced Vibration of Circular Cylindrical Structures.* Hemisphere.

Chen, S. S. & Wambsganss, W. 1972 Parallel-flow-induced vibrations of fuel rods. *Nuclear Engng and Design* **18**, 253–278.

Christopherson, D. & Naylor, H. 1955 Experiments on a wire moving in a tube filled with viscous fluid. *Proc. Inst. Mech. Engng* **35**, 169–184.

Eifler, W. & Nijsing, R. 1971 Berechnung der turbulenten Geschwindigkeitsverteilung und Wandreibung in exzentrischen Ringspalten. *Atomkernenergie* **18**, 133–142.

Gauthier, M. 1995 *Desk Edition, Handbook, ASM Interantional.* The Materials Information Society.

Geering, H. 1990 *Mess-und Regelungstechnik*, 2nd Edn. Springer.

Hu, H. H. & Joseph, D. D. 1989 Lubricated pipelining. Stability of core-annular flow. Part 2. *J. Fluid Mech.* **205**, 359–396.

Huang, A., Christodoulou, C. & Joseph, D. D. 1994 Friction factor and holdup studies for lubricated pipelining – II: Laminar and k-ε models of eccentric core flow. *Intl J. Multiphase Flow* **20**, 481–491.

Indelkofer, H. 1981 Zur Frage des Formbeiwertes und der Überlagerung von Rauhigkeitseinflüssen, erläutert am Beispiel der Ringspaltströmung. In *Mitteilungen Institut für Wasserbau und Wasserwirtschaft*, vol. 35, pp. 5–84. Rouvé, G., Aachen.

Jonsson, V. K. 1966 Experiments on turbulent-flow phenomena in eccentric annular ducts. *J. Fluid Mech.* **25**, 65–86.

Koch, R. & Feind, K. 1958 Druckverlust und Wärmeübergang in Ringspalten. *Chemie Ing. Techn.* **9**, 577–584.

Krause, H. W. 1988 *Textil-Technik, Grundzüge-Vorlesung.* Inst. für Textilmaschinenbau und Textilindustrie, ETH Zürich.

Lüscher, P., Wintermantel, E. & Annen, M. 1995 A new injectable open-porous implant system. *21st Annual Meeting of the Society for Biomaterials, San Francisco, California, USA.*

Meirovitch, L. 1986 *Elements of Vibration Analysis*, 2nd Edn. McGraw-Hill.

Nelson, A. R. & Robertson, J. M. 1968 Analytical studies of turbulent friction in annular conduits. *T & AM Rep.* 321, Dep. of Theor. and Appl. Mechanics, University of Illinois.

Ooms, G. 1972 The hydrodynamic stability of core-annular flow of two ideal liquids. *Appl. Sci. Res.* **26**, 147–158.

Ooms, G., Segal, A. & Van Der Wees, A. 1984 A theoretical model for core-annular flow of a very viscous oil core and a water annulus through a horizontal pipe. *Intl J. Multiphase Flow* **10**, 41–60.

Paidoussis, M. P. 1966*a* Dynamics of flexible slender cylinders in axial flow. Part 1. Theory. *J. Fluid Mech.* **26**, 717–736.

Paidoussis, M. P. 1966*b* Dynamics of flexible slender cylinders in axial flow. Part 2. Experiments. *J. Fluid Mech.* **26**, 737–751.

Paidoussis, M. P. 1973 Dynamics of cylindrical structures subjected to axial flow. *J. Sound Vib.* **29**, 365–385.

Paidoussis, M. P. & Pettigrew, M. J. 1979 Dynamics of flexible cylinders in axisymmetrically confined axial flow. *J. Appl. Mech.* **46**, 37–44.

Piercy, N., Hooper, M. & Winny, H. 1933 Viscous flow through pipes with cores. *Phil. Mag.* (7) **15**, 647–676.

Redberger, P. & Charles, M. 1962 Axial laminar flow in a circular pipe containing a fixed core. *Can. J. Chem. Engng* Aug. 148–151.

RSB 1996 NIH Image, http://rsb.info.nih.gov/nih-image/, Research Service Branch of the National Institute of Mental Health, U. S. National Institutes of Health, Springfield, Virginia.

Sabit, A. & Mohamed, M. H. 1991 Analysis of air flow in air-jet filling insertion. *Textile Res. J.* May, 253–256.

Schlichting, H. & Gersten, K. 1997 *Grenzschicht-Theorie*, 9th Edn. Springer.

Secomb, T. W. & El-Kareh, A. W. 1994 A model for motion and sedimentation of cylindrical red-cell aggregates during slow blood flow in narrow horizontal tubes. *J. Biomech. Engng* **116**, 243–261.

Shigechi, T., Kawae, N. & Lee, Y. 1990 Turbulent fluid flow and heat transfer in concentric annuli with moving cores. *Intl J. Heat Mass Transfer* **33**, 2029–2037.

Shigechi, T., Momoki, S. & Lee, Y. 1994 Fully developed laminar flow and heat transfer in eccentric annuli with axially moving cores. *Fund. Heat Transfer Forced Convection, ASME, Heat Transfer Div.* **285**, 75–84.

Shigechi, T. & Lee, Y. 1991 An analysis on fully developed laminar fluid flow and heat transfer in concentric annuli with moving cores. *Intl J. Heat Mass Transfer* **34**, 2593–2601.

Snyder, W. T. & Goldstein, G. A. 1965 An analysis of fully developed laminar flow in an eccentric annulus. *AIChE J.* **11**, 462–467.

Tiedt, W. 1968 Berechnung des laminaren und turbulenten Reibungswiderstandes konzentrischer und exzentrischer Ringspalten, Nr. 4. *Technischer Bericht aus dem Institut für Hydrologie der Technischen Hochschule Darmstadt*.

Vaskopulos, T., Polymeropoulos, C. E. & Zebib, A. 1993 Heat transfer from optical fibre during the draw process. *J. Mat. Proc. Manuf. Sci.* **1**, 261–271.

Wambsganss, M. W. & Chen, S. S. 1971, Tentative design guide for calculating the vibration response of flexible cylindrical elements in axial flow. *ANL-ETD* 71-07, Argonne National Laboratory, Illinois.